Understanding CO oxidation reaction on platinum nanoparticles

Rosa M. Arán-Ais, Francisco J. Vidal-Iglesias, Manuel J.S. Farias, José Solla-Gullón, Vicente Montiel, Enrique Herrero, Juan M. Feliu

PII: S1572-6657(16)30489-1
DOI: doi: 10.1016/j.jelechem.2016.09.031
Reference: JEAC 2845

To appear in: *Journal of Electroanalytical Chemistry*

Received date: 26 July 2016
Revised date: 20 September 2016
Accepted date: 21 September 2016

Please cite this article as: Rosa M. Arán-Ais, Francisco J. Vidal-Iglesias, Manuel J.S. Farias, José Solla-Gullón, Vicente Montiel, Enrique Herrero, Juan M. Feliu, Understanding CO oxidation reaction on platinum nanoparticles, *Journal of Electroanalytical Chemistry* (2016), doi: 10.1016/j.jelechem.2016.09.031

Understanding CO oxidation reaction on platinum nanoparticles

Rosa M. Arán-Ais[1], Francisco J. Vidal-Iglesias[1], Manuel J. S. Farias[2], José Solla-Gullón[1], Vicente Montiel[1], Enrique Herrero[1] and Juan M. Feliu[1]**

[1]Instituto de Electroquímica, Universidad de Alicante, Ap. 99, E-03080 Alicante, Spain.

[2]Departamento de Química, Universidade Federal do Maranhão, Avenida dos Portugueses, 1966, CEP 65080-805, São Luís - MA, Brazil

*Corresponding authors e-mail: herrero@ua.es, juan.feliu@ua.es

Abstract

To understand how the CO oxidation reaction proceeds on nanoparticles, which have complex surface structures, the behavior of the nanoparticles for the reaction has to be related to that of single crystal electrodes with a well-defined surface structure. However, the direct extrapolation of the results is not possible because significant differences in the behavior between both type of surfaces are observed. In single crystal electrodes in both acidic and alkaline media, the reaction initiates on defects on the CO adlayer. These defects can be already present on the surface, as surface defects or steps, or generated during the formation of the CO adlayer. In the case of steps, the oxidation starts on the lower part of the step. The only difference between the reaction behavior between acidic and alkaline solutions is the lower mobility of the CO in alkaline solutions, which generates adlayers with higher number of defects and give rise to multiple stripping peaks in stepped surfaces. Using these results, the differences of the behavior between single crystal electrodes and nanoparticles can be rationalized. In spite of the fact that nanoparticles have small ordered domains, the presence of sites in which the reaction is initiated, equivalent to the site in the lower part of the step, is almost negligible, and thus, the oxidation reaction takes place at higher potential values

than in stepped surfaces with similar domain size. Also the effect of nanoparticle agglomeration in the oxidation has been rationalized.

1. Introduction

The electrooxidation of CO on platinum (Pt) is a widely studied reaction. Its importance is due to its common presence as poison species in many electrochemical reactions, mainly produced during the oxidation of organic molecules or fuels. In addition, CO is also present in hydrogen used as fuel coming from reforming processes. During its oxidation, the CO molecules together with oxygenated species have to be previously adsorbed at the surface of the catalyst, and thus the surface structure of the Pt surface plays an important role by strongly controlling the catalyst reactivity. In fact this reaction is extremely sensitive towards the surface structure and there is a vast bibliography in which this subject is addressed [1-7]. Due to its importance, CO oxidation has been extensively studied with well-defined surfaces, especially at Pt single crystals both in acid and alkaline media. In addition, and from a more applied point of view, previous attempts have been made to compare the behavior of Pt nanoparticles with that of Pt single crystals by using shape-controlled nanoparticles. In this sense, many synthetic routes have been developed over the past years to obtain Pt nanomaterials [8-17]. Regarding the electrochemical characterization of Pt surfaces, this type of studies has been mainly performed in acid medium. It is important to bear in mind that for this purpose, it has to be considered that the nanoparticles are not perfect surfaces, showing different type of sites on their surfaces. In addition, and unlike single crystal basal planes, which present ideal infinite terraces, nanoparticles possess shorter and narrower ordered domains. Even in the case of stepped surfaces where the width of the terrace is controlled, the length of the terrace is ideally infinite. The first manuscript where CO oxidation was evaluated with shape-controlled nanoparticles was reported by

Solla-Gullón et al. and a clear dependence was observed between the CO oxidation electrocatalytic properties and the presence of bidimensional (100) and (111) domains at the surface of the nanoparticles [18]. Later, Brimaud et al. also performed a similar study reaching similar conclusions [19]. In these studies with nanoparticles, the observed voltammograms for CO oxidation show two main peaks, being that centered at a higher potential (around 0.77 V vs RHE) related to CO oxidation at (100) domains. Unfortunately, the behavior in alkaline medium is not as easily explained as in acid medium and similar behaviors were reported for nanoparticles with different shapes [20]. In addition, for nanoparticle systems, the study becomes even more complicated, as agglomeration effects have to be also considered. In this sense, it was reported for acid medium that for quasi-spherical nanoparticles deposited on carbon with low metal loading (10%), a single CO oxidation peak was reported [21]. However, when this percentage was increased another peak was clearly observed at lower potential. This effect was ascribed to an inter-particle interaction where CO and OH species could be adsorbed on different nanoparticles, similarly to what was described for Pt and Ru [22]. On the contrary, in alkaline medium no difference for aggregated nanoparticles was reported [20].

In this manuscript, CO oxidation on Pt single crystals is reviewed and used as a tool to understand this reaction on shape-controlled nanoparticles in acidic and alkaline media, with the aim of identifying the common features in the behavior in both media and to explain the differences. In addition, the agglomeration effect by using supported and non-supported nanoparticles is also considered.

2. Experimental

2.1. Reagents

Platinum(II) acetylacetonate ($Pt(acac)_2$, 97 %), oleylamine (OLA, 70 %), oleic acid (OA, 90 %), benzyl ether (BE, 98 %), tungsten hexacarbonyl ($W(CO)_6$, 99.99 %) and manganese (0) carbonyl ($Mn_2(CO)_{10}$, 98 %) were purchased from Sigma-Aldrich. Sodium hydroxide (NaOH, p.a.) was obtained from Merck. Methanol, ethanol and acetone (Reag. Ph. Eur) were purchased from Panreac, chloroform from J. T. Baker, and n-hexane (96 %) from Scharlau. All the chemicals were used as received without further purification.

2.2. Synthesis and cleaning of shaped Pt nanoparticles

Synthesis of Pt nanoparticles with preferential cubic truncated shape ($PtNP_{trunc}$) was performed using the method described by Y. Kang et al. [23], and those with a preferential cubic shape ($PtNP_{cubic}$) following a modified version of the methodology reported by J. Zhang et al. [12]. In both types of synthesis, OLA and OA are used as capping agents and metal carbonyls as additives. Briefly, $PtNP_{trunc}$ were obtained by dissolving Pt precursor (80 mg) in 10 mL of BE, 7.36 mL of OLA, and 1.25 mL of OA. The mixture was loaded into a three-neck flask equipped with a condenser. The mixture was mildly stirred under an argon stream and the reaction flask was heated. A solution of 8 mg of $Mn_2(CO)_{10}$ in 1 mL of chloroform was injected into the precursor mixture at 160 ºC, and the reaction temperature was in the range of 190-210 ºC. After 30 min of reaction, the solution was cooled down and the product was isolated by adding ethanol and by centrifugation. The nanocrystals were redispersed in hexane.

$PtNP_{cubic}$ were synthesized by dissolving 60 mg of $Pt(acac)_2$ and 150 mg of $W(CO)_6$ in 24 mL of OLA, and 6 mL of OA. The mixture was loaded into a Teflon-lined

stainless-steel autoclave (50 mL) and kept under argon atmosphere. The sealed autoclave was then placed into a preheated (180 ºC) oil bath. The oil bath temperature was in the range of 165-170 ºC. After 3 hours of reaction, cubic faceted Pt nanocrystals were obtained. The resulting solution was naturally cooled down to room temperature, the product was isolated by adding ethanol and by centrifugation and finally redispersed in hexane.

The different suspensions of Pt shaped nanoparticles in hexane were added into a dispersion of carbon (Vulcan XC72R) in hexane. The mixtures were intermittently stirred and ultrasonicated at room temperature for 3 h, and aged overnight. The Pt/C suspensions were precipitated by adding ethanol and further centrifugation. The resulting supported nanoparticles were washed following the method described in a previous work [24, 25], which has been demonstrated to effectively remove the capping agents OLA/OA from the nanoparticles without perturbing their surface structure. In brief, the precipitates were dispersed in 40.0 mL of methanol and 2 pellets of NaOH (about 0.4 g) were added to the dispersion, which was sonicated for 5 minutes. The supported nanoparticles were allowed to naturally precipitate overnight. Then, the alkaline solution of methanol was removed and the particles were washed with acetone. This procedure, using methanol+NaOH/acetone, was repeated three times. Finally, the catalyst was washed 3 times with ethanol, filtered and dried for 30 min in an oven at 70 ºC.

2.3. Material Characterization

Transmission electron microscopy (TEM) measurements were performed with a JEOL JEM-2010 microscope working at 200 kV and with a JEOL JEM-1400 Plus working at 120 kV. The samples were prepared by placing a drop of the hexane

suspension onto a Formvar-covered copper grid and drying it in air at room temperature. For each sample, usually about 200–300 particles from different parts of the grid were used to estimate the mean diameter and size distribution of the nanoparticles. Thermogravimetric analysis (TGA, Mettler-Toledo TGA/SDTA851 thermobalance) was used to determine the Pt loading (% in weight) of the prepared carbon supported Pt nanoparticles. Typically, a known mass of catalyst was heated from 25 to 850 °C at a heating rate of 10 °C min^{-1} in a N_2:O_2 (4:1) atmosphere. The Pt loading for the $PtNP_{trunc}$ and $PtNP_{cubic}$ were 24.4 % and 22.4 %, respectively.

2.4. Electrochemical surface characterization

The electrochemical characterization of the different Pt shaped nanoparticles was performed at room temperature by cyclic voltammetry at a sweep rate of 50 mV s^{-1} in Ar (Air Liquide, N50) saturated 0.5 M H_2SO_4 (96 %, Merck, Suprapur®), 0.1 M $HClO_4$ (70 %, Merck, Suprapur®) and 0.1 M NaOH (99.99 %, Merck, Suprapur®) solutions. A three-electrode electrochemical cell was used with a Pt wire as a counter electrode and a reversible hydrogen electrode (RHE), connected to the cell through a Luggin capillary, as reference electrode. The electrode potential was controlled using a VMP3 multichannel potentiostat (BioLogic) with a NStat configuration (1 counter electrode, 1 reference electrode and 4 working electrodes working simultaneously). Unsupported nanoparticles were deposited on a gold collector, while carbon supported nanocatalysts were deposited onto a glassy carbon rod. Before every experiment, both types of collectors were polished with alumina and rinsed with ultra-pure water to eliminate the nanoparticles from previous essays. A droplet of the nanoparticle suspension was pipetted onto the polished substrates and the solvent was allowed to evaporate in an Ar atmosphere. The determination of the active surface area of the different Pt

nanoparticles was performed in H_2SO_4 by the charge involved in the so-called hydrogen under potential deposition (H_{upd}) region, assuming 230 μC cm^{-2} for the total charge after the subtraction of the double layer charging contribution, as previously discussed [20]. CO oxidation experiments were carried out by bubbling CO (g) (N47, Air Liquide) through the electrolyte at 0.1 V until complete blockage of the surface, which was monitored by cycling the electrode between 0.05 and 0.3 V. After that, CO was removed from the solution by bubbling Ar for at least 20 min and CO stripping voltammograms were performed at 20 mV s^{-1} in order to oxidize the CO molecules adsorbed on the surface in a single sweep.

3. Results

3.1.CO oxidation on Pt single crystals in acidic media.

As aforementioned, for a better understanding of the CO oxidation mechanism on nanoparticles, which present a complicated surface structure, it is important to determine the oxidation mechanism on Pt single crystal electrodes. For this type of electrodes, the surface structure is precisely controlled, so that clear correlations between the surface structure and the observed reactivity could be established. Additionally the simplification of the surface structure provides an excellent ground where different models for kinetics could be tested.

The simplest surface in which the oxidation can be tested is the Pt(111) electrode, because this surface has only one type of site with hexagonal symmetry and it is the most compact surface structure, with the lowest surface energy. For this reason, it is normally addressed in DFT calculations, allowing a comparison between experimental results and theoretical models and providing a better understanding of the oxidation process. The first element that should be taken into account when the CO oxidation is

addressed is the CO adsorption mode and structures on the surface. On Pt(111) electrodes in acidic solutions, adsorbed CO forms ordered surface structures, depending on the CO coverage and adsorption conditions. As revealed by in situ scanning tunneling microscopy (STM) and X-ray diffraction (XRD), in the presence of CO in solution a (2×2)-θ_{CO}=0.75 structure is formed [26-31] (figure 1). In ultra-high vacuum (UHV), the maximum attained coverage is 0.50 [32], which reveals the important role of water and/or, the surface charge in the formation of the CO adlayer (in addition to the presence of abundant CO at the interphase). In this sense, the water structure in contact with electrode surface is modified by the presence of CO, indicating a clear interaction between both species [33]. It should be noted that this structure is only stable in the presence of CO in solution [34, 35] and when CO is removed from solution this structure is transformed into a (√19×√19) R23.4°-θ_{CO}=0.68 [34, 36] (figure 1). At lower CO coverages, a (√7×√7) R19.1°-θ_{CO}=0.56 structure could also be detected [34].

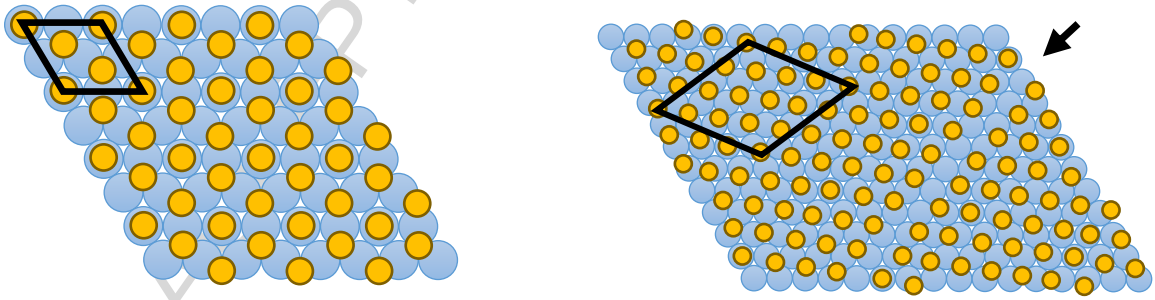

Figure 1. CO adlayer structures on Pt(111) electrodes. The right panel shows two translational domains and the defects in the adlayer created on the borders of the two domains (marked by the arrow).

When a saturated CO adlayer on a Pt(111) electrode is oxidized on the surface, it was shown that the peak potential for the CO stripping (figure 2) was affected by the number of defects [37, 38] and the electrode potential at which the CO adlayer was formed [38]. In fact, a significant shift to lower potential values in the peak potential is observed when the number of defects is increased, even when they are well below 1%,

that is, when they are almost undetectable in the cyclic voltammetry of the electrode [37]. As can be seen, when CO is present in the solution, the onset for the CO oxidation is displaced ca. 0.12 V to higher potential values. This shift is due to two main reasons. First, in the presence of CO a more compact (2×2)-Θ_{CO}=0.75 adlayer is formed so that the initiation process is hindered and second, the presence of CO in solution assists in the healing process when defects are created in the adlayer in the initial oxidation stages [39].

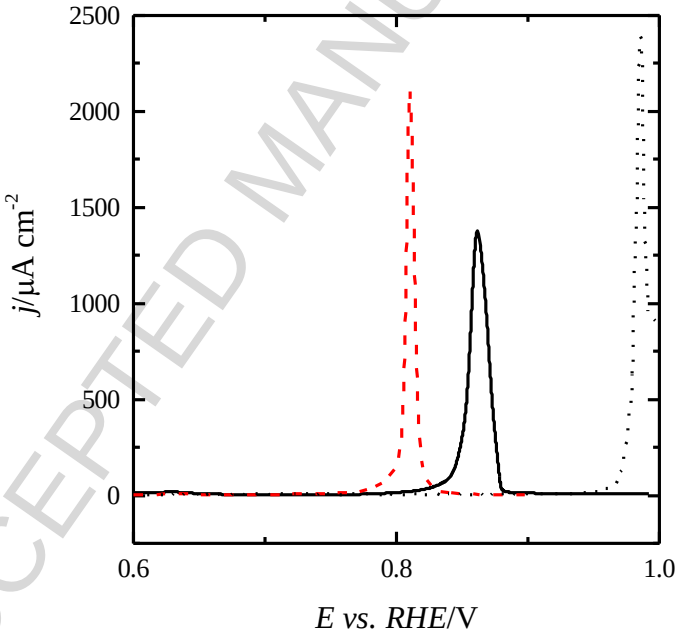

Figure 2. CO stripping profile for the Pt(111) (full black line) and Pt(776) (dashed red line) electrodes in 0.5 M H_2SO_4. The dotted black line represents the positive scan direction for Pt(111) electrode in a saturated CO solution in a rotating disk arrangement at 600 rpm. Scan rate: 50 mV s^{-1}.

When the kinetics of the chronoamperometric transients for CO oxidation using non saturation coverages obtained using the impinging jet system were analyzed [40], it was shown that the transients could be fitted with a mean field Langmuir-Hinselwood (L-H) mechanism according to the expression:

$$j = nFk(E)\theta_{CO}(1-\theta_{CO})$$

where *k(E)* is the rate constant of the reaction, which depends on the electrode potential, θ_{CO} is the CO coverage and $(1-\theta_{CO})$ represents the free sites where OH adsorption can take place. In this mechanism, the oxidation occurs between an adsorbed CO molecule and adsorbed OH in a non-covered-by-CO Pt site. The very good fitting with mean field mechanism (figure 3) implies that the mobility of CO is large, so that a random distribution of the adsorbed CO and adsorbed OH is found at all times [41]. If the mobility of CO molecules were low, the oxidation mechanism would have taken place according to a nucleation and growth L-H mechanism, which would have had transients with a different shape. This model was also used to fit the voltammetric stripping peaks [39, 42] and also the oxidation of solution bulk CO [39] providing an excellent agreement between the experimental results and the model. From this model, it was clear that the number of defects present both on the electrode surface and on the CO adlayer plays a very important role in triggering the oxidation process.

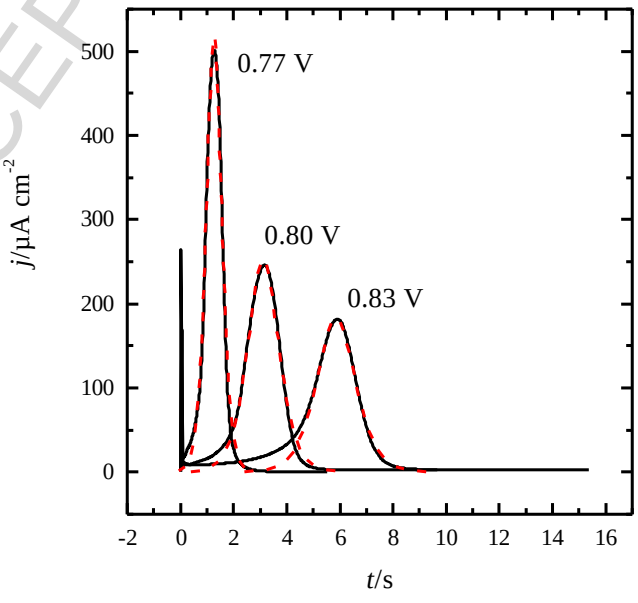

Figure 3. Chronoampeometic profiles for CO stripping on a Pt(322) electrode in 0.5 M H_2SO_4 at three different potentials. The dashed line represents the fitting according to the mean field L-H mechanism.

A controlled and precise way to study the role of defects in the oxidation process is the use of stepped surfaces. In a stepped surface, the infinite two-dimensional terrace is perturbed periodically by the presence of a monoatomic step with a known symmetry. By changing the step density of the surface and the symmetry of the step, the effect of these steps or terrace defects can be quantitatively analyzed. When the Pt(111) surface is modified by the presence of steps, a significant change takes place in the CO oxidation process. Essentially, the oxidation is catalyzed by the presence of the steps, so that the peak potential is displaced towards negative values as the step density increases (figure 2) [5], in agreement with the results obtained with Pt(111) electrodes with different amount of surface defects [37]. When the kinetics of the process at the stepped surfaces was analyzed, it was found that the reaction rate for the oxidation at a given potential is directly proportional to the step density. Moreover, the extrapolation of the results obtained with the stepped surfaces to an ideal defect-free Pt(111) surface would indicate that the oxidation rate on this surface would be negligible in comparison with that measured on stepped surfaces [4, 43]. This result again highlights the role of defects in the oxidation mechanism and is in agreement with a mean-filed L-H mechanism. In this type of mechanism, OH should adsorb on the electrode surface and the only place where this adsorption can take place is around a defect. These defects can be already present on the initial (111) surface, as in the case of steps, or be created on the CO adalyer. It should be noted that the different CO ordered adlayers present several rotational and translational domains, so different patches with the different rotational and translational domains can appear on the surface (see figure 1), as revealed by in situ STM [34]. The borders of those patches, which are defects on the CO structure, can act as initiation sites for OH adsorption on the surface.

For these stepped surfaces, partial CO coverages also provide valuable information on the mechanism of the process. These coverages can be obtained either by controlled dosing of CO or by partial stripping of a full CO monolayer. It is well known that distinct signals from adsorption process on step and terrace sites appear on the voltammetric profile of the stepped surfaces in the supporting electrolyte. Thus, controlling the CO dosing rate on the surface to obtain partial coverages allows the preferential adsorption site for CO to be determined. When these experiments are performed either in potentiostatic or potentiodinamic conditions, it was observed that the initial stages of CO adsorption takes place both on terrace and step sites, although the deposition rate on the steps is higher than that measured for the terrace [44], and the step is fully covered before the adsorption process on the terrace is finished. However, DFT calculations clearly indicate that the adsorption energy on the step site is ca. 0.4 eV higher than that calculated on the terrace site [45] and the site located in the lower part of the step has the lowest adsorption energy. This would suggest that the adsorption of CO should take place on the steps before occurring on the terrace, and that the terrace occupancy would progress from the top part of the step. The difference between the experimental results and the calculations probably arises from the presence of important lateral repulsive interactions between CO molecules, modifying the energetics of the process during the adsorption [34]. Initially, CO molecules would adsorb on distant step sites, so that lateral interactions between the adsorbed CO molecules are negligible. When all these sites are covered, adsorption would take place on terrace sites not close to those previously occupied to avoid lateral interactions with other adsorbed CO molecules, as shown in figure 4A. When all these sites are covered, the adsorption would take place again on the step site, because under these conditions, it is still the most favorable site, (figure 4B). As the coverage increases, steps become completely

covered and finally a saturation coverage is reached, where all sites are blocked (figure 4C).

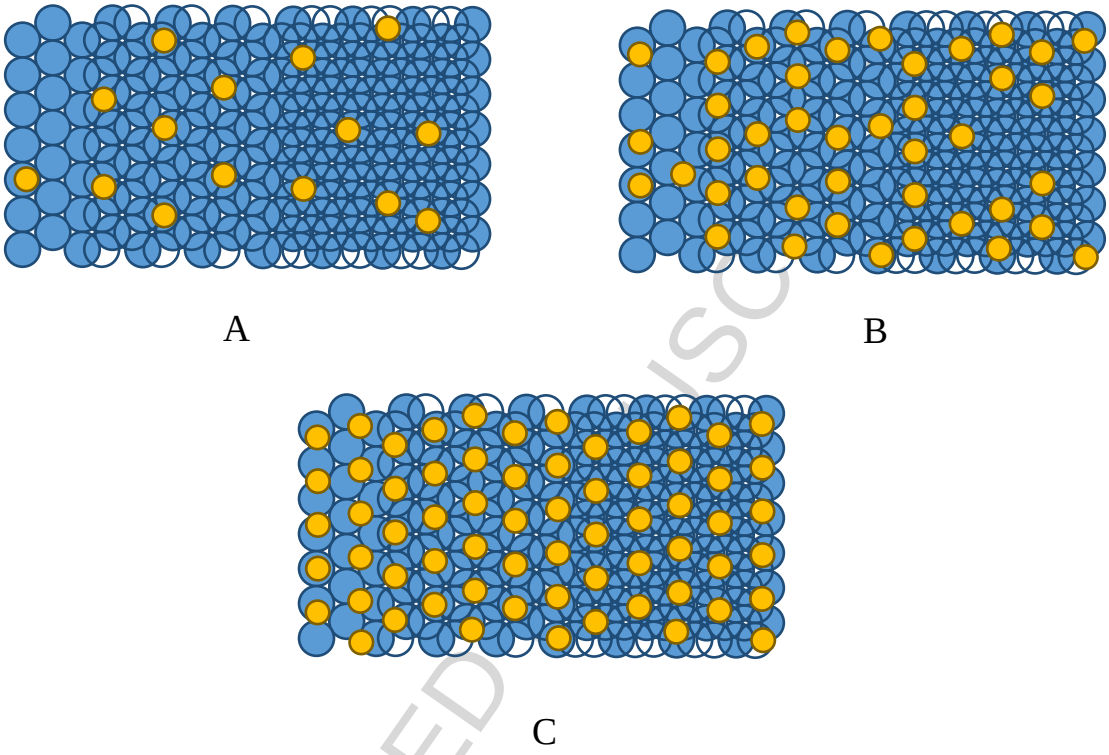

Figure 4. Scheme with evolution of the CO adlayer structures of a stepped surface with (111) symmetry terrace as the CO coverage increases: A) low coverages, B) intermediate coverages and C) saturation coverages.

On the other hand, when the partial coverages are obtained from partial stripping of the CO adlayer, the oxidation takes place initially on the terrace, since the peaks related to the adsorption of hydrogen on the steps are not observed until all CO molecules adsorbed on terrace sites have been oxidized. These initial situations correspond to figures 5A and B. Finally, the last sites to be freed are those corresponding to the step sites, which agree with the higher adsorption energy of CO on the step site [45, 46] (figure 5C).

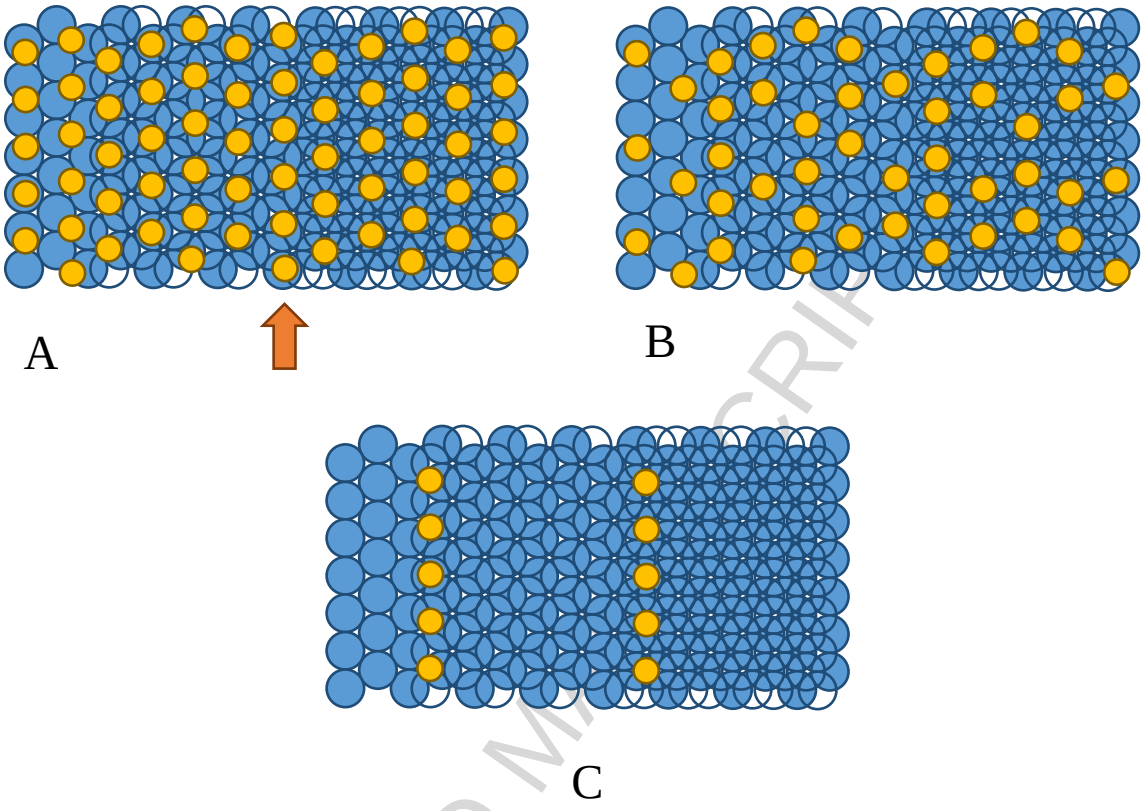

Figure 5. Scheme with the evolution of the CO adlayer on a stepped surface with (111) symmetry terrace as the oxidation progresses in acidic solutions: A) Initial CO adlayer. The arrow indicates the row of CO molecules where the oxidation starts. B) Intermediate coverages. C) Last stage in the oxidation process.

Adatom decoration of the step sites has also been used to get further insights into the oxidation process of CO on these surfaces. Two different behaviors have been described according to the oxophilic character of the deposited adatom [47, 48]. It should be noted that the tested adatoms are preferentially deposited on the lower site of the step, due to the favorable energetics of this site for the adsorption of these adatoms [46, 49-51]. When the step is decorated with Bi or Te, which do not adsorb oxygen species at the CO oxidation potentials [52-54], the oxidation rate diminishes, revealing the important role of the lower part of the step in the oxidation mechanism [47, 55]. For these decorated stepped surfaces, the kinetics still follows the mean field L-H mechanism. On the other hand, on Ru decorated stepped surfaces a significant catalytic effect is observed [48]. Moreover, one voltammetric peak at ca. 0.5 V is observed when

the step is fully decorated, whereas up to three peaks at 0.50, 0.56 and 0.62 V are observed for partial decorations. This important catalytic effect should be related to the adsorption of OH on Ru, acting as a bifunctional catalyst. It should be noted that the potentials for CO oxidation on the Ru decorated surfaces are lower than those that are recorded on Pt electrodes, even at very low CO coverages. At very low CO coverages, OH can be adsorbed easier on the Pt surface, expediting the oxidation reaction. For these coverages, CO stripping gives rise to a peak at ca. 0.7 V [56]. The even lower potential on Ru decorated surfaces clearly indicates the active role of Ru on the oxidation mechanism providing adsorbed OH at low potentials.

For Pt(100) and Pt(110) and its stepped surfaces the number of studies are significantly lower. However, the whole picture described for the (111) vicinal surfaces are still applicable. Thus, the presence of local defects in the CO adlayer on a (100) surface or the addition of monoatomic steps, catalyzes the oxidation of CO [57] and the kinetics follow a mean field L-H mechanism [42, 58].

All these results with the low index and stepped surfaces allow suggesting an oxidation mechanism for CO, which explains the observed behavior. Clearly, the oxidation initiates on defect points present on the adlayer. In an ideal Pt(111) surface, the defects would be located at the borders of the rotational and translational domains present on the CO adlayer, as shown in figure 1. On these sites, OH adsorption can easily occur, initiating the oxidation process. It is proposed that CO molecules have a large mobility on Pt surfaces in acidic solutions, since the oxidation kinetics are easily reproduced with a mean-field L-H mechanism. Thus, as the oxidation proceeds, the CO adlayer relaxes and provides new sites on the terrace for the adsorption of additional OH species, accelerating the reaction up to its completion. On stepped surfaces, thus, the presence of the step already creates the defects in the CO adlayer necessary to initiate

the reaction. Thus, the initial site would be the lower part of the step, because it is the site with the lowest adsorption energy for CO and it is in the border of the domain of the CO adlayer. This row of sites is marked with an arrow in figure 5A. On some of these sites, OH would adsorb initiating the reaction and then accelerating it. The last molecules, in this case, to be oxidized are those located on top of the step. The voltammograms after partial stripping indicate that this is the last site that is released in the oxidation process. The decoration of the step by Bi or Te diminishes the reaction rate, because it affects the initiation step in the oxidation, resulting in a small decrease of the reaction rate.

The situation in which Ru decorates the step is different. As aforementioned, due to the oxophilicity of Ru, it acts as a bifunctional catalyst, providing the sites where OH adsorption takes place at low potentials. When the step is fully decorated, the OH adsorbed on Ru starts the oxidation process on the CO molecules that are on the top of the step, because CO and OH can directly interact. Once these molecules have been oxidized, the top sites are repopulated by incoming CO molecules from terrace sites and oxidizing the whole CO adlayer in a single peak. For partial Ru decoration, the potential at which OH is adsorbed on the decorating Ru adatoms will depend on the number of Ru nearest neighbors. Isolated Ru adatoms will adsorb OH at more positive potentials, justifying the peak multiplicity for CO oxidation at a partial decorated step.

3.2.CO oxidation on Pt nanoparticles in acidic media.

In principle, the oxidation of CO on Pt nanoparticles should follow the same trends as those observed on the single crystal electrodes. However, experimental results indicate that the correlation is not as simple as it would appear. Additionally, it has been observed that not only the surface structure of the nanoparticles affects the oxidation

behavior, but also the agglomeration of the nanoparticles [21, 59]. As will be shown later, the close contact of nanoparticles leads to lower onset and peak potentials for the CO stripping peak. To understand better these effects, preferentially shaped nanoparticles have been used. Cubic and cube-octahedral nanoparticles, that is, nanoparticles that preferentially have (100) and a mixture of (100) and (111) domains are used in this study. These two types of nanoparticles have been studied in two different conditions: they have been deposited on a gold substrate, so that agglomeration occurs, and also they have been dispersed on a carbon support, on which they can be considered as isolated. The electrochemical behavior of these samples for CO oxidation will allow understanding the effect of the surface structure and dispersion of the catalyst on the support.

Figure 6 shows the TEM images of the different samples of nanoparticles unsupported and supported on the carbon. As can be easily seen, nanoparticles have a cubic shape and, when are deposited on the carbon support, they are well dispersed. The cyclic voltammetries of the samples in sulfuric and perchloric acid solutions (figure 7) allow a better characterization of the samples. First, from the different signals present on the sample, it allows assessing the presence of ordered domains. As has been extensively documented in H_2SO_4 medium [20, 60] the presence of large (100) ordered domains leads to signals at 0.37 V, whereas a signal between 0.4 and 0.6 V is characteristic of sulfate adsorption on (111) domains. Additionally, it can be seen that those signals are not affected by the presence of the support. The only difference between the voltammograms is the appearance of a large double layer contribution from the carbon support (both carbon black and glassy carbon contributions). In addition, the observed differences between the supported vs unsupported responses of the samples are due to the distinct amount of nanoparticles deposited. In any case, the constancy in

the voltammetric profile assures that the integrity on the nanoparticles is maintained upon dispersion on the carbon and that the effects of the carbon support on the electronic structure of the nanoparticles can be considered negligible.

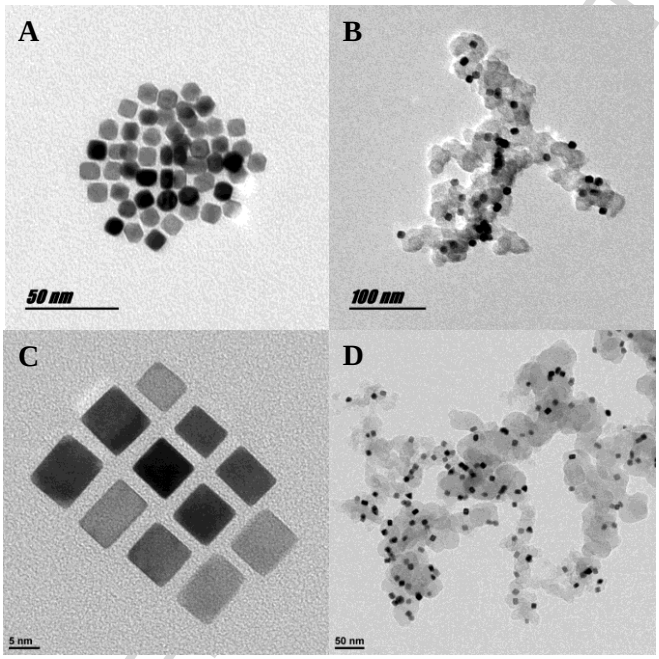

Figure 6. TEM images of the (A,B) cube-octahedral and (C,D) cubic nanoparticles. B and D samples have been dispersed on carbon.

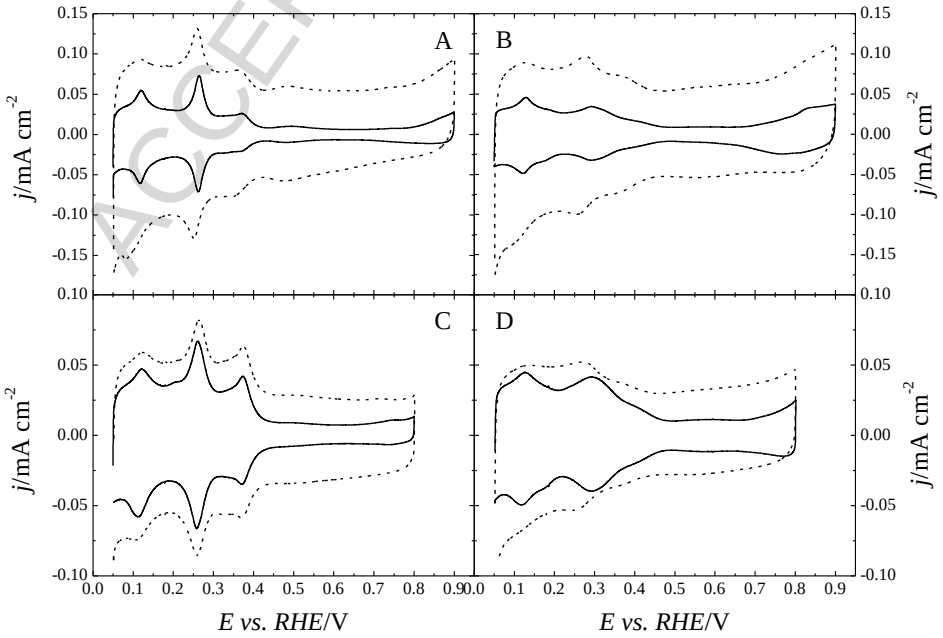

Figure 7. Voltammetric profiles of the supported (dashed line) and unsupported (solid line) (A, B) cube-octahedral and (C, D) cubic nanoparticles in (A, C) 0.5 M sulfuric acid and (B, D) 0.1 M perchloric acid solutions. Scan rate: 50 mV s^{-1}.

The CO stripping voltammetries of the nanoparticles in the two supporting electrolytes can be seen in figure 8. As observed with single crystal electrodes, the stripping peak in sulfuric acid solutions takes place at higher potential values [42, 61], as a consequence of the adsorption of sulfate, that hinders OH adsorption on the surface. Another important feature in the voltammetric profile is the presence of sharp peaks at higher potentials in the voltammograms of the unsupported nanoparticles. These sharp peaks are associated with the presence of ordered domains [62]. As has been observed with single crystal electrodes in these media [42], the peaks for the (111) domains appear at potentials higher than the corresponding to the (100) domains. Additionally, it is corroborated that the dispersion of the nanoparticles leads to an important shift of the peak potentials of ca. 25-100 mV, depending on the sample. Thus, the presence of aggregated nanoparticles affects the CO oxidation process.

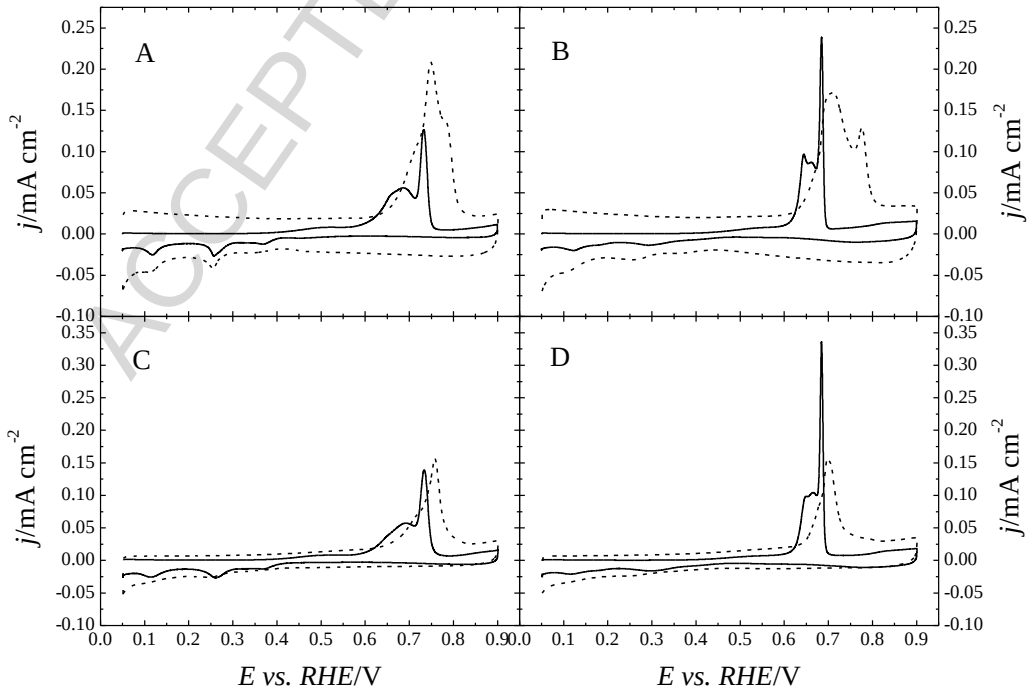

Figure 8. CO stripping voltammetric profiles of the supported (dashed line) and unsupported (solid line) (A, B) cube-octahedral and (C, D) cubic nanoparticles in (A, C) 0.5 M sulfuric acid and (B, D) 0.1 M perchloric acid solutions. Scan rate: 20 mV s^{-1}.

The behavior of these nanoparticles can be now compared with that observed for the single crystal electrodes. It should be noted that the size of the expected ordered (111) and (100) domains on the nanoparticles correspond to that present on short (111) or (100) terraces. However, the peak potentials for the CO stripping peak are higher than those corresponding to these stepped surfaces. The difference can be easily understood when the initiation mechanism of the oxidation on the stepped surfaces is considered. In the stepped surfaces, the oxidation begins on the lower part of the step, and this type of site is not present in perfect cubic or cube-octahedral nanoparticles. On the surface of these nanoparticles, the ordered domains are completely surrounded by edges, which are the analogous sites to the top part of the step, on which CO adsorption is stronger than inside the terrace. There are no lower parts, where CO adsorption is weaker and the initiation process is easier. Thus, the initiation process is retarded in comparison with that observed on the equivalent stepped surfaces, leading to higher peak potentials. When two nanoparticles are close together, in the place where the two nanoparticles are in contact, a defect in the CO adlayer will appear, so that, OH adsorption is easier close to those sites and thus, oxidation process takes place at lower potential values. This *interparticle effect* justifies the lower peak potential for the agglomerated nanoparticles.

3.3.CO oxidation on Pt single crystals in alkaline media.

Although the general behavior of CO oxidation on platinum electrodes in alkaline media seems to follow the same principle than those observed in acidic solutions, a detailed inspection shows significant differences between both media. The first one is the presence of a prewave at lower potential values in the CO stripping voltammograms, whose appearance depends on the electrode potential at which the CO adlayer is formed

[63-68]. Thus, when the CO adlayer is formed in acidic solutions and then the electrode is transferred to alkaline media, the prewave is absent from the voltammetric profiles.

The second, and probably the most important difference is that several peaks appear in the stripping voltammogram for the stepped and kinked surfaces containing (111) terraces [65, 67-74]. Only one peak appears for the low index planes and stepped surfaces with (100) terraces, but for the (111) stepped surfaces, there are three characteristic peaks that can be clearly associated with the presence of (110) steps (or kinks) at ca. 0.55 V, (100) steps at ca. 0.7 V and (111) terraces at ca. 0.8 V (figure 9). Those potentials are almost independent of the size of the terrace [65].

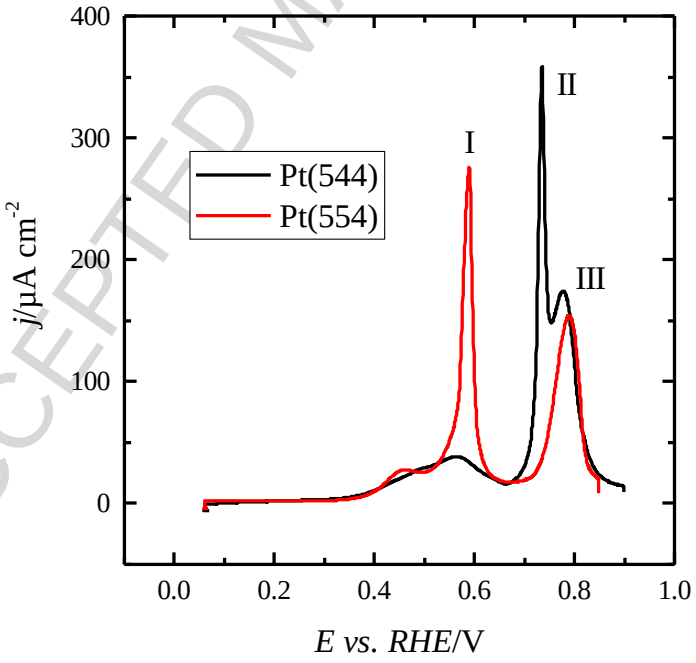

Figure 9. CO stripping profile for the Pt(544) and Pt(554) electrodes in 0.1 M NaOH. Scan rate: 50 mV s^{-1}. Peak I, is associated with the presence of (110) steps or kinks, peak II with the presence of (100) steps and III with the (111) terraces.

In the same way that done in acidic solutions, CO partial coverages obtained by partial stripping, revealed that the last site to be released is that corresponding to the top part of the step and these CO molecules are oxidized at 0.8 V [67, 71] (figure 10C). On

the other hand, the peaks at lower potentials, (those related to the presence of steps) are only observed when the adlayer is reaching saturation coverages [67]. Since peaks at lower potential values appear always when steps or kinks are present on the surface, the sites involved in the peaks at lower potential values should be those located on the lower part of the step. Thus, the CO oxidation process starts in the lower part of the step as marked by the arrow in figure 10A, giving rise to the peaks at lower potential values (peaks I or II in figure 9, depending on the symmetry of the step site). The rest of the CO molecules located on the terrace sites and those on the top part of the step are oxidized in the peak at ca. 0.8 V (peak III in figure 9).

Although the sites where the CO oxidation process starts are the same in acidic and alkaline solutions, the appearance of several peaks in this latter medium reveals differences in the kinetics, which are better studied in chronoamperometric experiments. The transients are more complex than those obtained in acidic solutions, and thus, the simple mean-field L-H mechanism with only two adjustable parameters does not fully reproduce the shape of the transients [65, 70]. In order to obtain reasonable fittings, models should include at least three parameters. Although, other explanations have been given [70, 71], probably the best fittings are obtained using a nucleation and growth model which takes into account the anisotropy created by the presence of the step [65]. The nucleation and growth model implies that the mobility of CO molecules is very low in alkaline medium. The estimated surface diffusion coefficient for CO in this medium is 2.7×10^{-20} m^2 s^{-1} [65].

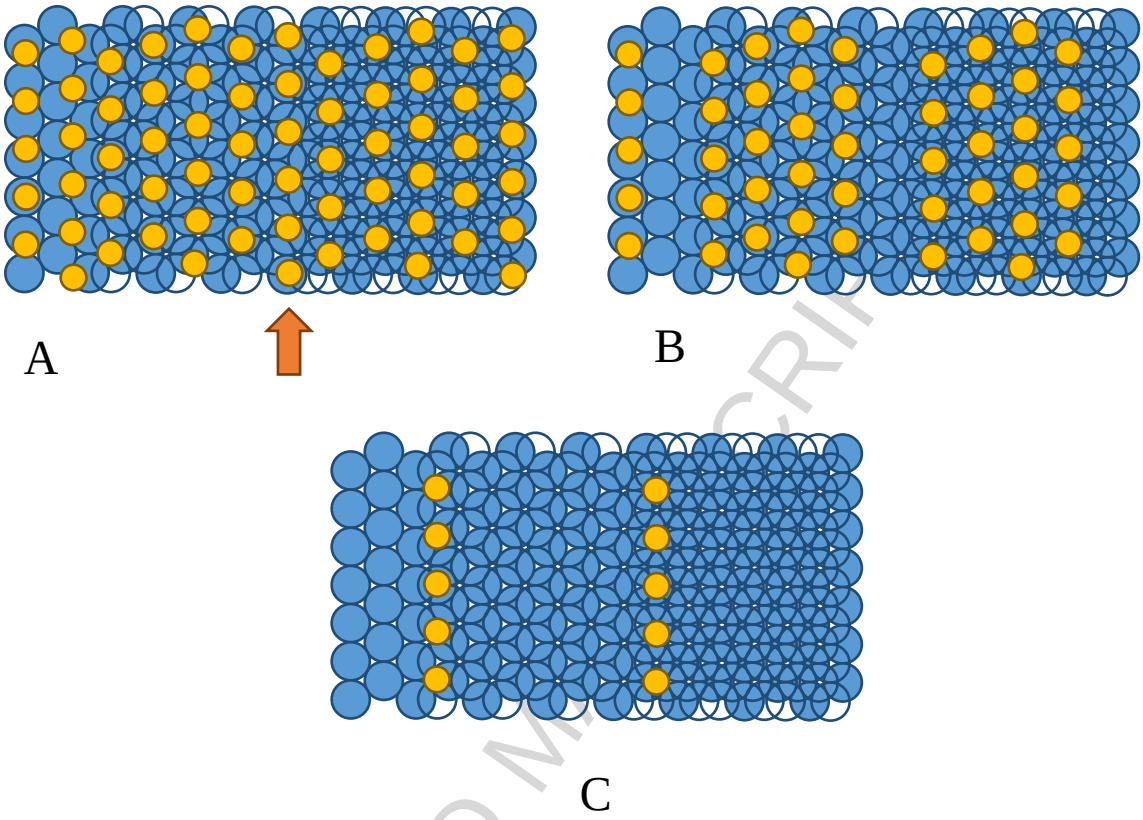

Figure 10. Scheme with the evolution of the CO adlayer on a stepped surface with (111) symmetry terrace as the oxidation progresses in alkaline solutions: A) Initial CO adlayer. The arrow indicates the row of CO molecules where the oxidation starts. B) Intermediate coverages. C) Last stage in the oxidation process.

This low mobility of CO serves to explain the differences of the stripping voltammogram in alkaline medium when compared to acidic solutions. In both media, the oxidation starts in the same sites, the lower part of the step (arrows in figures 5A and 10A), which are the most active sites for the oxidation. In acidic solutions, CO molecules are mobile and immediately repopulate these sites, where the oxidation of CO is easier (figure 5B), and thus the oxidation takes place in a single peak. In alkaline medium, it is proposed that the mobility of CO is very low. Thus, once the oxidation of the CO molecules in the lower part of the step is finished (those molecules are marked with the arrow in figure 10A and give rise to the peak at low potentials), the rest of the

molecules are oxidized at the corresponding potential for the terrace sites (figure 10B and C), originating the peak at higher potential values.

The low mobility also explains the appearance of prewaves. When the adlayer is formed in acidic conditions, the high mobility of the CO molecules help in the coalescence of the different domains formed in the initial stages of CO adsorption. The adlayer, thus, has lower defects, and there is no place to initiate the oxidation of the adlayer. In contrast, the low mobility of the CO in alkaline solutions gives rise to the formation of a very defective adlayer, where the initial stages of the oxidation take place. Although the origin of the low mobility of CO in alkaline medium is not clear, it has been proposed that the different water structure and/or the surface charge of the electrode may play a role in this process [68].

3.4. CO oxidation on Pt nanoparticles in alkaline media.

Figure 11 shows the voltammetric profiles of the nanoparticles in alkaline solutions, showing the characteristic signals assigned to the different sites present on the surfaces of the different nanoparticle samples [20]. As before, the only effect of the addition of a carbon support is the increase in the apparent double layer in the voltammogram, due to the carbon contribution. The stripping voltammogram of the CO adlayer in the unsupported and carbon-supported nanoparticles is also presented in figure 11. As can be seen, unlike the observed behavior due to agglomeration in acidic solution, the effects of the support in the CO stripping voltammetry are almost negligible. An additional characteristic of the voltammograms is that they contain, aside from the prevawe, a shoulder at low potentials followed by a peak at higher potentials. The general shape is almost independent of the shape of the nanoparticles, although the ratio of the different peaks and the exact peak position depends on the specific shape [75]. It

should be highlighted that the peaks associated with the steps on the (111) terraces are absent in the voltammetric profile, even when (111) domains are present on the surface of the nanoparticles. Again, the reason is the same to that given in acidic conditions to the presence of peaks at high potentials. The peaks at lower potentials in alkaline solutions and the catalysis of the oxidation is related to the lower part of the step, and this type of site is not present on the convex shape of the nanoparticle, where (111) domains are connected to other domains by a series of low coordinated atoms. Thus, the lack of those sites justifies the absence of the characteristic peaks of the (111) stepped surfaces.

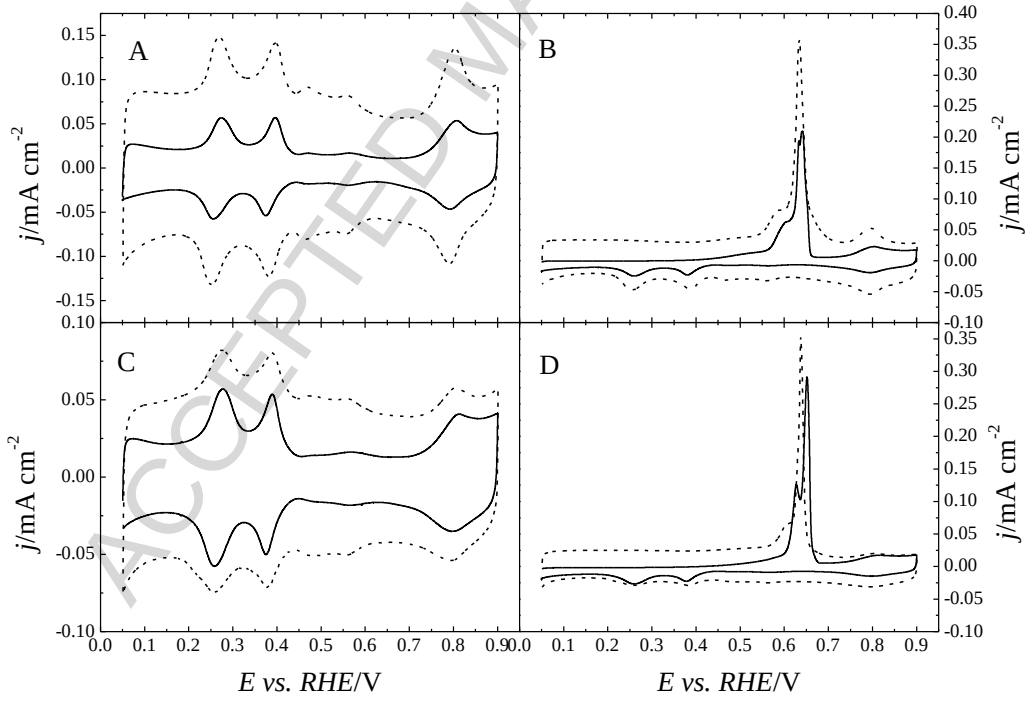

Figure 11. Voltammetric profiles of the supported (dashed line) and unsupported (solid line) (A) cube-octahedral and (C) cubic nanoparticles in 0.1 M NaOH at 50 mV s^{-1}. CO stripping voltammetric profiles of the supported (dashed line) and unsupported (solid line) (B) cube-octahedral and (D) cubic nanoparticles in 0.1 M NaOH at 20 mV s^{-1}.

Another difference with the acidic conditions is the small effect of the support in the stripping voltammogram. In absence of support, the nanoparticles agglomerate, giving rise to CO adlayers, in acidic solutions, with a large number of defects. In alkaline

solutions, since the adlayer has been formed at more negative potentials and it already contains a large number of defects, even for dispersed nanoparticles, the agglomeration does not result in a larger number of defects where the oxidation of the CO adlayer could start.

Finally, the presence of two peaks is the result of a nucleation and growth model. As the effect of different scan rates and partial stripping indicates [75], both peaks are interconnected. Peak potentials have the same scan rate dependence. Also, after partial stripping, when the scan direction is reversed at 0.65 V, the stripping peak in the next scan appears at lower potentials (figure 12). Clearly, both peaks are interconnected and have a common origin. Thus, the peak at lower potentials should be ascribed to the initial nucleation process to create the first holes in the adlayer, whereas the second one is related to the growth of the oxidation process. For this reason, if the scan is reversed after the first peak, the second peak appears at lower potentials in the following scan, since the nucleation event has already taken place, and the oxidation process in the following scan becomes easier.

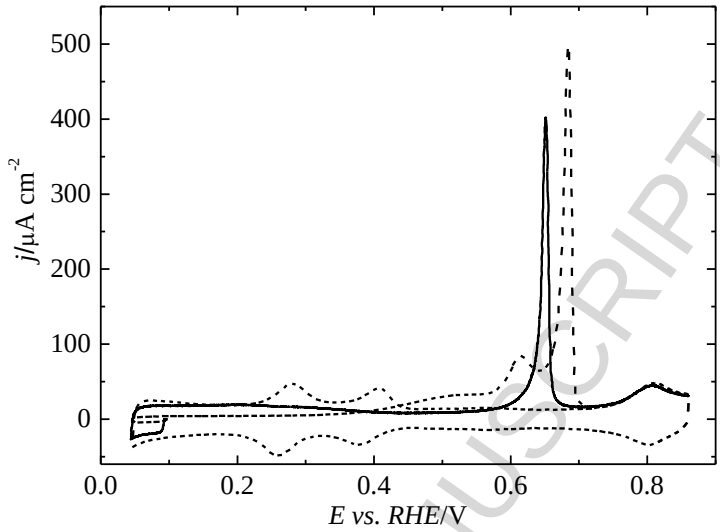

Figure 12. Voltammetric profile of a CO layer obtained after partial CO stripping up to 0.65 V on unsupported cubic nanoparticles in 0.1 M NaOH at 50 mV s^{-1}. The dashed line represents the stripping profile of a full CO layer on the same nanoparticles.

Conclusions

Although the voltammetric behavior of the CO oxidation reaction in acidic and alkaline solutions has very distinct features, the only significant difference in the reaction mechanism is the low mobility of CO on the electrode surface in alkaline solutions. Aside from that, the reaction proceeds using a common mechanism. The reaction is initiated by defects in the CO adlayer. When the origin of these defects is the presence of a surface defect or step, the active site is the lower part of the defect. As this type of site is not present at the surface of the nanoparticles, the CO oxidation reaction on nanoparticles occurs at higher potential values than in stepped surfaces. Additionally, in alkaline solutions, the access of the CO molecules to the most active sites is hindered by the low mobility of CO, which also contributes to higher oxidation potentials.

Acknowledgements.

This work has been financially supported by the MCINN-FEDER (projects CTQ 2013-44083-P and CTQ2013-48280-C3-3-R) and Generalitat Valenciana (project PROMETEO/2014/013). M.J.S. Farias acknowledges financial support from the CAPES (Brazil) for financial support.

References.

[1] J.M. Feliu, J.M. Orts, A. Fernández-Vega, A. Aldaz, J. Clavilier, Electrochemical studies in sulphuric acid solutions of adsorbed CO on Pt (111) electrodes J. Electroanal. Chem., 296 (1990) 191-201.

[2] E. Herrero, J.M. Feliu, A. Aldaz, Poison formation reaction from formic acid on Pt(100) electrodes modified by irreversibly adsorbed bismuth and antimony J. Electroanal. Chem., 368 (1994) 101-108.

[3] J.M. Leger, B. Beden, C. Lamy, S. Bilmes, Carbon-Monoxide Electrosorption on Low Index Platinum Single-Crystal Electrodes, J. Electroanal. Chem., 170 (1984) 305-317.

[4] N.P. Lebedeva, M.T.M. Koper, J.M. Feliu, R.A. van Santen, Role of crystalline defects in electrocatalysis: Mechanism and kinetics of CO adlayer oxidation on stepped platinum electrodes, J. Phys. Chem. B, 106 (2002) 12938-12947.

[5] N.P. Lebedeva, M.T.M. Koper, E. Herrero, J.M. Feliu, R.A. van Santen, CO oxidation on stepped Pt n(111) x (111) electrodes, J. Electroanal. Chem., 487 (2000) 37-44.

[6] K.J.J. Mayrhofer, M. Arenz, B.B. Blizanac, V. Stamenkovic, P.N. Ross, N.M. Markovic, CO surface electrochemistry on Pt-nanoparticles: A selective review, Electrochim. Acta, 50 (2005) 5144-5154.

[7] M.T.M. Koper, S.C.S. Lai, E. Herrero, Mechanisms of the Oxidation of Carbon Monoxide and Small Organic Molecules at Metal Electrodes, in: M.T.M. Koper (Ed.) Fuel Cell Catalysis, A Surface Science Approach, John Wiley & Sons, Inc, Hoboken, NJ, 2009, pp. 159-208.

[8] T.S. Ahmadi, Z.L. Wang, T.C. Green, A. Henglein, M.A. El-Sayed, Shape-controlled synthesis of colloidal platinum nanoparticles, Science, 272 (1996) 1924-1926.

[9] C. Burda, X. Chen, R. Narayanan, M.A. El-Sayed, Chemistry and properties of nanocrystals of different shapes, Chem. Rev., 105 (2005) 1025-1102.

[10] A.R. Tao, S. Habas, P. Yang, Shape control of colloidal metal nanocrystals, Small, 4 (2008) 310-325.

[11] Y. Xia, Y. Xiong, B. Lim, S.E. Skrabalak, Shape-controlled synthesis of metal nanocrystals: Simple chemistry meets complex physics?, Angew. Chem. Int. Ed., 48 (2009) 60-103.

[12] J. Zhang, J. Fang, A general strategy for preparation of Pt 3d-transition metal (Co, Fe, Ni) nanocubes, J. Am. Chem. Soc., 131 (2009) 18543-18547.

[13] L. Wang, Y. Yamauchi, Metallic Nanocages: Synthesis of Bimetallic Pt–Pd Hollow Nanoparticles with Dendritic Shells by Selective Chemical Etching, J. Am. Chem. Soc., 135 (2013) 16762-16765.

[14] H. Ataee-Esfahani, M. Imura, Y. Yamauchi, All-Metal Mesoporous Nanocolloids: Solution-Phase Synthesis of Core–Shell Pd@Pt Nanoparticles with a Designed Concave Surface, Angew. Chem. Int. Ed., 52 (2013) 13611-13615.

[15] G.J. Leong, M.C. Schulze, M.B. Strand, D. Maloney, S.L. Frisco, H.N. Dinh, B. Pivovar, R.M. Richards, Shape-directed platinum nanoparticle synthesis: Nanoscale design of novel catalysts, Appl. Organomet. Chem., 28 (2014) 1-17.

[16] Y. Li, B.P. Bastakoti, V. Malgras, C. Li, J. Tang, J.H. Kim, Y. Yamauchi, Polymeric Micelle Assembly for the Smart Synthesis of Mesoporous Platinum Nanospheres with Tunable Pore Sizes, Angew. Chem. Int. Ed., 54 (2015) 11073-11077.

[17] Z. Wu, S. Yang, W. Wu, Shape control of inorganic nanoparticles from solution, Nanoscale, 8 (2016) 1237-1259.

[18] J. Solla-Gullón, F.J. Vidal-Iglesias, E. Herrero, J.M. Feliu, A. Aldaz, CO monolayer oxidation on semi-spherical and preferentially oriented (100) and (111) platinum nanoparticles, Electrochem. Commun., 8 (2006) 189-194.

[19] S. Brimaud, S. Pronier, C. Coutanceau, J.M. Léger, New findings on CO electrooxidation at platinum nanoparticle surfaces, Electrochem. Commun., 10 (2008) 1703-1707.

[20] F.J. Vidal-Iglesias, R.M. Arán-Ais, J. Solla-Gullon, E. Herrero, J.M. Feliu, Electrochemical Characterization of Shape-Controlled Pt Nanoparticles in Different Supporting Electrolytes, ACS Catal., 2 (2012) 901-910.

[21] A. López-Cudero, J. Solla-Gullón, E. Herrero, A. Aldaz, J.M. Feliu, CO electrooxidation on carbon supported platinum nanoparticles: Effect of aggregation, J. Electroanal. Chem., 644 (2010) 117-126.

[22] L. Zhuang, J. Jin, H.D. Abruña, Direct Observation of Electrocatalytic Synergy, J. Am. Chem. Soc., 129 (2007) 11033-11035.

[23] Y. Kang, J.B. Pyo, X. Ye, R.E. Diaz, T.R. Gordon, E.A. Stach, C.B. Murray, Shape-controlled synthesis of pt nanocrystals: The role of metal carbonyls, ACS Nano, 7 (2013) 645-653.

[24] R.M. Arán-Ais, F.J. Vidal-Iglesias, J. Solla-Gullon, E. Herrero, J.M. Feliu, Electrochemical characterization of clean shape-controlled Pt nanoparticles prepared in presence of oleylamine/oleic acid, Electroanalysis, 27 (2015) 945-956.

[25] R.M. Arán-Ais, J. Solla-Gullón, M. Gocyla, M. Heggen, R.E. Dunin-Borkowski, P. Strasser, E. Herrero, J.M. Feliu, The effect of interfacial pH on the surface atomic elemental distribution and on the catalytic reactivity of shape-selected bimetallic nanoparticles towards oxygen reduction, Nano Energy, 27 (2016) 390-401.

[26] I. Villegas, M.J. Weaver, Carbon monoxide adlayer structures on platinum (111) electrodes: A synergy between in-situ scanning tunneling microscopy and infrared spectroscopy, J. Chem. Phys., 101 (1994) 1648-1660.

[27] I. Oda, J. Inukai, M. Ito, Compression structures of carbon-monoxide on a Pt(111) electrode surface studied by in situ scanning tunneling microscopy, Chem. Phys. Lett., 203 (1993) 99-103.

[28] C.A. Lucas, N.M. Markovic, P.N. Ross, The adsorption and oxidation of carbon monoxide at the Pt(111)/electrolyte interface: atomic structure and surface relaxation, Surf. Sci., 425 (1999) L381-L386.

[29] N.M. Markovic, B.N. Grgur, C.A. Lucas, P.N. Ross, Electrooxidation of CO and H2/CO mixtures on Pt(111) in acid solutions, J. Phys. Chem. B, 103 (1999) 487-495.

[30] K.C. Chang, A. Menzel, V. Komanicky, H. You, Electrosorbed carbon monoxide monolayers on Pt(111), Electrochim. Acta, 52 (2007) 5749-5758.

[31] J.X. Wang, I.K. Robinson, B.M. Ocko, R.R. Adzic, Adsorbate-geometry specific subsurface relaxation in the CO/Pt(111) system, J. Phys. Chem. B, 109 (2005) 24-26.

[32] M.J. Weaver, S.C. Chang, L.W.H. Leung, X. Jiang, M. Rubel, M. Szklarczyk, D. Zurawski, A. Wieckowski, Evaluation of absolute saturation coverages of carbon monoxide on ordered low-index platinum and rhodium electrodes J. Electroanal. Chem., 327 (1992) 247-260.

[33] A. Yamakata, M. Osawa, Dynamics of Double-Layer Restructuring on a Platinum Electrode covered by CO: Laser-Induced Potential Transient Measurement, J. Phys. Chem. C, 112 (2008) 11427-11432.

[34] I. Villegas, M.J. Weaver, Carbon-monoxide adlayer structures on platinum(111) electrodes - a synergy between in-situ scanning-tunneling-microscopy and infrared-spectroscopy, J. Chem. Phys., 101 (1994) 1648-1660.

[35] A. Rodes, R. Gómez, J.M. Feliu, M.J. Weaver, Sensitivity of compressed carbon monoxide adlayers on platinum(III) electrodes to long-range substrate structure: Influence of monoatomic steps, Langmuir, 16 (2000) 811-816.

[36] Y.V. Tolmachev, A. Menzel, A.V. Tkachuk, Y.S. Chu, H.D. You, In situ surface X-ray scattering observation of long-range ordered (root 19 x root 19)R23.4 degrees-13CO structure on Pt(111) in aqueous electrolytes, Electrochem. Solid-State Lett., 7 (2004) E23-E26.

[37] N.P. Lebedeva, M.T.M. Koper, J.M. Feliu, R.A. van Santen, The effect of the cooling atmosphere in the preparation of flame-annealed Pt(111) electrodes on CO adlayer oxidation, Electrochem. Commun., 2 (2000) 487-490.

[38] A. López-Cudero, A. Cuesta, C. Gutiérrez, Potential dependence of the saturation CO coverage of Pt electrodes: The origin of the pre-peak in CO-stripping voltammograms. Part 1: Pt(1 1 1), J. Electroanal. Chem., 579 (2005) 1-12.

[39] C.A. Angelucci, E. Herrero, J.M. Feliu, Modeling CO Oxidation on Pt(111) Electrodes, J. Phys. Chem. C, 114 (2010) 14154-14163.

[40] M. Bergelin, E. Herrero, J.M. Feliu, M. Wasberg, Oxidation of CO adlayers on Pt(111) at low potentials: an impinging jet study in H2SO4 electrolyte with mathematical modeling of the current transients, J. Electroanal. Chem., 467 (1999) 74-84.

[41] A.V. Petukhov, W. Akemann, K.A. Friedrich, U. Stimming, Kinetics of electrooxidation of a CO monolayer at the platinum/electrolyte interface, Surf. Sci., 402 (1998) 182-186.

[42] E. Herrero, B. Alvarez, J.M. Feliu, S. Blais, Z. Radovic-Hrapovic, G. Jerkiewicz, Temperature dependence of the COads oxidation process on Pt(111) Pt(100), and Pt(110) electrodes, J. Electroanal. Chem., 567 (2004) 139-149.

[43] M.T.M. Koper, N.P. Lebedeva, C.G.M. Hermse, Dynamics of CO at the solid/liquid interface studied by modeling and simulation of CO electro-oxidation on Pt and PtRu electrodes, Faraday Discuss., 121 (2002) 301-311.

[44] M.J.S. Farias, A.A. Tanaka, G. Tremiliosi, J.M. Feliu, On the apparent lack of preferential site occupancy and electrooxidation of CO adsorbed at low coverage onto stepped platinum surfaces, Electrochem. Commun., 13 (2011) 338-341.

[45] C. Buso-Rogero, E. Herrero, J. Bandlow, A. Comas-Vives, T. Jacob, CO oxidation on stepped-Pt(111) under electrochemical conditions: insights from theory and experiment, Phys. Chem. Chem. Phys., 15 (2013) 18671-18677.

[46] A. Ferre-Vilaplana, R. Gisbert, E. Herrero, On the electrochemical properties of platinum stepped surfaces vicinal to the (100) pole. A computational study, Electrochim. Acta, 125 (2014) 666-673.

[47] Q.S. Chen, A. Berna, V. Climent, S.G. Sun, J.M. Feliu, Specific reactivity of step sites towards CO adsorption and oxidation on platinum single crystals vicinal to Pt(111), Phys. Chem. Chem. Phys., 12 (2010) 11407-11416.

[48] M.J.S. Farias, W. Cheuquepan, G.A. Camara, J.M. Feliu, Disentangling Catalytic Activity at Terrace and Step Sites on Selectively Ru-Modified Well-Ordered Pt Surfaces Probed by CO Electro-oxidation, ACS Catal., 6 (2016) 2997-3007.

[49] E. Herrero, V. Climent, J.M. Feliu, On the different adsorption behavior of bismuth, sulfur, selenium and tellurium on a Pt(775) stepped surface, Electrochem. Commun., 2 (2000) 636-640.

[50] V. Del Colle, A. Berna, G. Tremiliosi, E. Herrero, J.M. Feliu, Ethanol electrooxidation onto stepped surfaces modified by Ru deposition: electrochemical and spectroscopic studies, Phys. Chem. Chem. Phys., 10 (2008) 3766-3773.

[51] G. Samjeske, X.Y. Xiao, H. Baltruschat, Ru decoration of stepped Pt single crystals and the role of the terrace width on the electrocatalytic CO oxidation, Langmuir, 18 (2002) 4659-4666.

[52] J. Clavilier, J.M. Feliu, A. Aldaz, An irreversible structure sensitive adsorption step in bismuth underpotential deposition at platinum electrodes, J. Electroanal. Chem., 243 (1988) 419-433.

[53] J. Clavilier, J.M. Feliu, A. Fernandezvega, A. Aldaz, Electrochemical-Behavior of Irreversibly Adsorbed Bismuth on Pt (100) with Different Degrees of Crystalline Surface Order, J. Electroanal. Chem., 269 (1989) 175-189.

[54] P. Rodríguez, E. Herrero, A. Aldaz, J.M. Feliu, Tellurium adatoms as an in-situ surface probe of (111) two-dimensional domains at platinum surfaces, Langmuir, 22 (2006) 10329-10337.

[55] Q.S. Chen, J.M. Feliu, A. Berna, V. Climent, S.G. Sun, Kinetic study of CO oxidation on step decorated Pt(111) vicinal single crystal electrodes, Electrochim. Acta, 56 (2011) 5993-6000.

[56] E. Herrero, A. Fernández-Vega, J.M. Feliu, A. Aldaz, Poison formation reaction from formic acid and methanol on Pt(111) electrodes modified by irreversibly adsorbed Bi and As J. Electroanal. Chem., 350 (1993) 73-88.

[57] K. Domke, E. Herrero, A. Rodes, J.M. Feliu, Determination of the potentials of zero total charge of Pt(100) stepped surfaces in the 01(-1) zone. Effect of the step density and anion adsorption, J. Electroanal. Chem., 552 (2003) 115-128.

[58] F.J. Vidal-Iglesias, J. Solla-Gullón, J.M. Campina, E. Herrero, A. Aldaz, J.M. Feliu, CO monolayer oxidation on stepped Pt(S) (n-1)(100) x (110) surfaces, Electrochim. Acta, 54 (2009) 4459-4466.

[59] F. Maillard, S. Schreier, M. Hanzlik, E.R. Savinova, S. Weinkauf, U. Stimming, Influence of particle agglomeration on the catalytic activity of carbon-supported Pt nanoparticles in CO monolayer oxidation, Phys. Chem. Chem. Phys., 7 (2005) 385-393.

[60] J. Solla-Gullón, P. Rodríguez, E. Herrero, A. Aldaz, J.M. Feliu, Surface characterization of platinum electrodes, Phys. Chem. Chem. Phys., 10 (2008) 1359-1373.

[61] S. Blais, G. Jerkiewicz, E. Herrero, J.M. Feliu, New insight into the electro-oxidation of the irreversibly chemisorbed bismuth on Pt(111) through temperature-dependent research, J. Electroanal. Chem., 519 (2002) 111-122.

[62] J. Solla-Gullón, F.J. Vidal-Iglesias, P. Rodríguez, E. Herrero, J.M. Feliu, A. Aldaz, Shape-dependent electrocatalysis: CO monolayer oxidation at platinum nanoparticles, 2005, pp. 1-11.

[63] J.S. Spendelow, G.Q. Lu, P.J.A. Kenis, A. Wieckowski, Electrooxidation of adsorbed CO on Pt(111) and Pt(111)/Ru in alkaline media and comparison with results from acidic media, J. Electroanal. Chem., 568 (2004) 215-224.

[64] J.S. Spendelow, J.D. Goodpaster, P.J.A. Kenis, A. Wieckowski, Mechanism of CO oxidation on Pt(111) in alkaline media, J. Phys. Chem. B, 110 (2006) 9545-9555.

[65] E. Herrero, Q.-S. Chen, J. Hernandez, S.-G. Sun, J.M. Feliu, Effects of the surface mobility on the oxidation of adsorbed CO on platinum electrodes in alkaline media. The role of the adlayer and surface defects, Phys. Chem. Chem. Phys., 13 (2011) 16762-16771.

[66] R.M. Arán-Ais, M.C. Figueiredo, F.J. Vidal-Iglesias, V. Climent, E. Herrero, J.M. Feliu, On the behavior of the Pt(100) and vicinal surfaces in alkaline media, Electrochim. Acta, 58 (2011) 184-192.

[67] M.J.S. Farias, E. Herrero, J.M. Feliu, Site Selectivity for CO Adsorption and Stripping on Stepped and Kinked Platinum Surfaces in Alkaline Medium, J. Phys. Chem. c, 117 (2013) 2903-2913.

[68] M.J.S. Farias, C. Buso-Rogero, R. Gisbert, E. Herrero, J.M. Feliu, Influence of the CO Adsorption Environment on Its Reactivity with (111) Terrace Sites in Stepped Pt Electrodes under Alkaline Media, J. Phys. Chem. C, 118 (2014) 1925-1934.

[69] G. Garcia, M.T.M. Koper, Stripping voltammetry of carbon monoxide oxidation on stepped platinum single-crystal electrodes in alkaline solution, Phys. Chem. Chem. Phys., 10 (2008) 3802-3811.

[70] G. Garcia, M.T.M. Koper, Mechanism of electro-oxidation of carbon monoxide on stepped platinum electrodes in alkaline media: a chronoamperometric and kinetic modeling study, Phys. Chem. Chem. Phys., 11 (2009) 11437-11446.

[71] G. Garcia, M.T.M. Koper, Dual Reactivity of Step-Bound Carbon Monoxide during Oxidation on a Stepped Platinum Electrode in Alkaline Media, J. Am. Chem. Soc., 131 (2009) 5384-5385.

[72] G. Garcia, P. Rodriguez, V. Rosca, M.T.M. Koper, Fourier Transform Infrared Spectroscopy Study of CO Electro-oxidation on Pt(111) in Alkaline Media, Langmuir, 25 (2009) 13661-13666.

[73] P. Rodríguez, G. García, E. Herrero, J. Feliu, M. Koper, Effect of the Surface Structure of Pt(100) and Pt(110) on the Oxidation of Carbon Monoxide in Alkaline Solution: an FTIR and Electrochemical Study, Electrocatalysis, 2 (2011) 242-253.

[74] G. García, M.T.M. Koper, Carbon monoxide oxidation on Pt single crystal electrodes: Understanding the catalysis for low temperature fuel cells, ChemPhysChem, 12 (2011) 2064-2072.

[75] M.J.S. Farias, F.J. Vidal-Iglesias, J. Sola-Gullon, E. Herrero, J.M. Feiu, On the behavior of CO oxidation on shape-controlled Pt nanoparticles in alkaline medium, J. Electroanal. Chem., 716 (2014) 16-22.